Novel modes of synchronization in star networks of coupled chemical oscillators

David Mersing[1],* Shannyn A. Tyler[1],† Benjamas Ponboonjaroenchai[1,2],‡ Mark R. Tinsley[1],§ and Kenneth Showalter[1]¶

[1] *C. Eugene Bennett Department of Chemistry, West Virginia University, Morgantown, WV 26506-6045 USA*

[2] *Department of Physics, Kasetsart University, Bangkok 10900, Thailand*

Abstract

Photochemically coupled micro-oscillators are studied experimentally and computationally in star networks to investigate the modes and mechanisms of synchronization. The micro-oscillators are catalyst-loaded beads that are placed in catalyst-free Belousov-Zhabotinsky (BZ) solutions. The properties of the photochemical coupling between the oscillators are determined by the composition of the BZ reaction mixtures and both excitatory coupling and inhibitory coupling are studied. Synchronization of peripheral oscillators coupled through a hub oscillator is exhibited at coupling strengths leading to novel modes of synchronization of the hub with the peripheral oscillators. A theoretical analysis provides insights into the mechanism of the synchronization. The heterogeneous peripheral oscillators have different phase velocities that give rise to a phase divergence; however, the perturbation from the hub acts to realign the phases by delaying the faster oscillators more than the slower oscillators.

* Electronic address: damersing@mix.wvu.edu

† Electronic address: shtyler@mix.wvu.edu

‡ Electronic address: bbenjee24@gmail.com

§ Electronic address: mark.tinsley@mail.wvu.edu

¶ Electronic address: kshowalt@wvu.edu

We study photochemically coupled Belousov-Zhabotinsky (BZ) micro-oscillators [1–7] to explore synchronization in star networks [8–12] in both excitatory and inhibitory systems. The BZ reaction has been used as a model system for biological oscillators because it is a relaxation oscillator [13, 14]. Many natural oscillators have relaxation-type dynamics and can respond in an excitatory (synchronizing) or inhibitory (desynchronizing) manner to a coupling perturbation. We describe experiments, simulations and analytical theory that provide a detailed characterization of synchronization in chemical oscillator networks. This characterization is applicable to a broad class of oscillator networks, including those in biological systems.

I. INTRODUCTION

The emergent dynamical behaviors and functionality of networks of coupled oscillatory biological cells, such as neurons or pancreatic beta cells, are dependent, in part, on the topological structure of the network [15–19]. Many types of structural connectivity have been explored in various model and experimental systems [2, 3, 20–22]. Examples include local vs. non-local coupling, small-world and scale-free networks. These have revealed a rich array of dynamical behaviors, such as synchronization, wave propagation, clustering and chimera states [2, 3, 16, 17].

A defining characteristic of scale free networks is that they have a subset of nodes, termed hubs, that are highly connected in comparison to other nodes in the network [23, 24]. These have been found to arise naturally in many biological, social and artificial systems. A star network serves as a motif of such networks consisting of a single hub connected to a number of peripheral oscillators [25]. The study of a network motif can reveal important dynamical properties of the larger networks that it characterizes. In the case of star network motifs, a number of interesting dynamical behaviors have been demonstrated, including (1) chimera states involving subsets of the peripheral oscillators showing different dynamical patterns [26], (2) remote synchronization involving synchronization of topologically disconnected elements [8–10], and (3) explosive synchronization in which there is an abrupt second order transition to synchronization [27, 28].

Much of the work in coupled star networks has focused on the Stewart-Landau os-

cillators or Kuramoto phase oscillators [8–10, 27, 28]. In contrast, many natural oscillators have relaxation-type dynamics. This fundamentally different oscillatory waveform can respond in an excitatory (synchronizing) or inhibitory (desynchronizing) manner to a coupling perturbation [29]. For example, in a natural network of neurons, excitatory coupling tends to promote synchronization of oscillators whereas inhibitory coupling promotes asynchronous irregular states [30, 31]. A more recent work extended the study of coupled star networks using oscillators more akin to such biological oscillators [32]. They carried out computational and experimental studies of water-in-oil Belousov-Zhabotinsky micro-droplets coupled using a reaction-diffusion mechanism. The work revealed out-of-phase synchronization between the peripheral nodes and the hub at intermediate coupling strengths, while at larger coupling strengths the hub's oscillatory dynamics were suppressed.

In this work, we extend the exploration of dynamical behaviors of Belousov-Zhabotinsky (BZ) relaxation oscillators coupled in a star network. Our system allows us to control both frequency distributions of the oscillators and the nature of the coupling. The Belousov-Zhabotinsky reaction involves the oxidation of an organic substrate in the presence of a metal catalyst [14]. The BZ system has been used as a model system for biological oscillators, owing to the relaxation form of its oscillations. The development of a photochemical micro-oscillator version of the BZ reaction has allowed the exploration of dynamical behaviors across a range of different network structures [1–7]. Recent work has demonstrated that the photochemical response of a BZ micro-oscillator to a perturbation can be varied from excitatory to inhibitory through systematic changes in the reaction mixture composition [1].

We utilize photochemically coupled BZ micro-oscillators to explore synchronization using both excitatory and inhibitory coupling in star networks. We report experimental as well as computational findings. The experimental system consists of chemical micro-oscillators prepared by loading a photosensitive catalyst onto cation exchange beads, which are then immersed in a catalyst-free BZ solution. Real-time, light-based feedback allows the development of a network of coupled oscillators. Selection of appropriate catalyst-free reaction mixtures yields either excitatory or inhibitory responses to the light-based coupling [1, 33, 34]. We utilize phase response curves for targeting reaction mixture compositions that yield responses of interest [1].

II. EXPERIMENTAL

Individual chemical micro-oscillators are produced by loading cation exchange beads (Dowex 50-100 mesh, radius = 150-200 μm) with the photosensitive tris(2,2'-bipyridyl) ruthenium catalyst $Ru(bpy)_3^{2+}$, which are then immersed in a catalyst-free BZ solution [1, 4, 5, 35]. The oscillators are illuminated with a constant light intensity ϕ_0 at 440 nm using a spatial light modulator (SLM), Fig. 1. During a chemical oscillation, the oxidation state of the catalyst cyclically changes between +2 and +3. This results in changes to the amount of light absorbed and transmitted, allowing the state of each micro-oscillator to be monitored in grayscale using a CCD camera. The photosensitive ruthenium catalyzed BZ reaction allows real-time coupling through changes in the illumination of a micro-oscillator based on the current states of the micro-oscillators within the network.

In this work, we focus on investigating star systems where there is significant natural period difference between the hub node and the peripheral nodes[12, 25]. Such hub driven behavior has been found in natural networks such as neuronal functional networks [12]. To achieve the period difference, two groups of micro-oscillators are loaded with different amounts of catalyst [1]. The peripheral oscillators have a catalyst concentration of 2.5×10^{-5} mol g^{-1}, giving a natural period range of 80-100 s, while the hub oscillators have a catalyst concentration of 8.36×10^{-6} mol g^{-1}, with a natural period range of 50-70 s. Small variations in the loading of the catalyst introduces a natural heterogeneity in both the peripheral and hub micro-oscillators.

A star network of coupled oscillators, as illustrated in Fig. 1, is implemented by illuminating each oscillator j with light intensity Φ_j according to

$$\Phi_j = \Phi_0 + \frac{K}{d} \sum_{i=1}^{N+1} A(g_i - g_j), \tag{1}$$

where Φ_0 is the background light intensity, K is the coupling strength, d is the degree of each node, A is the adjacency matrix, and g_i and g_j are the normalized gray levels of oscillators i and j. In this work, $N + 1 = 6$, for the hub and the five peripheral oscillators. The response of an oscillator to changes in light intensity is dependent upon the composition of the catalyst-free BZ solution.

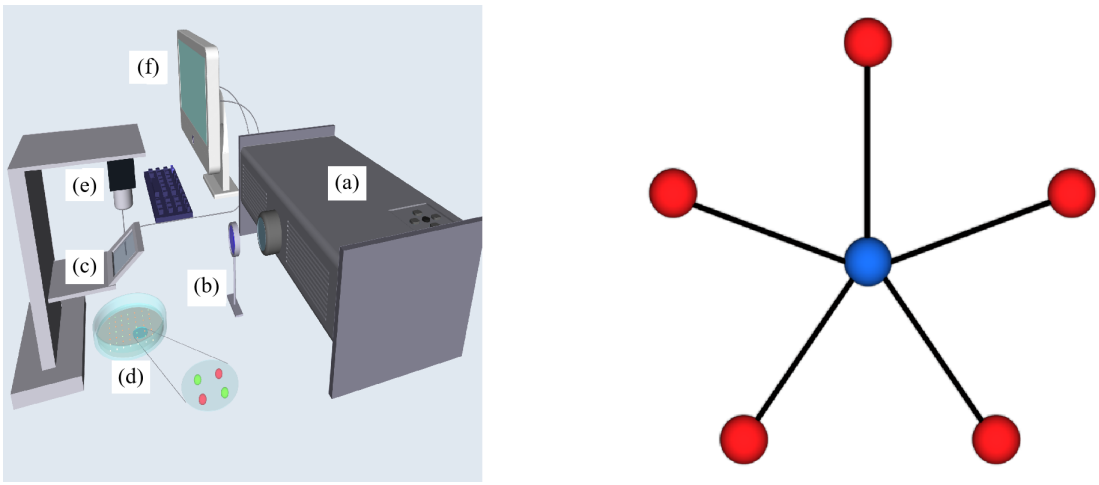

FIG. 1. Experimental setup shown in left panel. The projector (a) transmits collimated light through a 440-460 nm band pass filter (b) to the beam splitter (c). The light is reflected down to the reactor (d) and back up to the CCD camera (e) positioned above. The image is processed by the computer (f) and the proper feedback is calculated and applied by the modified projector. The right panel shows a star network of oscillators with 5 peripheral nodes. When constructing a given star network in an experiment, a set of 5 peripheral oscillators is selected that have a maximum difference in period of approximately 2%.

A. BZ Photochemistry

A BZ oscillation profile has the pulse-like characteristic of a relaxation oscillator, with a long, slow quiescent region of high inhibitor concentration, followed by a short, rapidly changing 'firing' region of autocatalytic growth of the activator [13, 14]. The firing is triggered when a critical ratio of activator, bromous acid, to inhibitor, bromide, is reached.

The photosensitive catalyst $Ru(bpy)_3^{2+}$ is excited by 440 nm light to form $Ru(bpy)_3^{2+*}$ [1–3]. Two potential mechanistic pathways then exist. The excitatory path involves the excited ruthenium complex reacting with bromate, BrO_3^-, to produce the autocatalyst bromous acid, $HBrO_2$:

$$Ru(bpy)_3^{2+*} + BrO_3^- + 2H^+ \rightarrow BrO_2^\bullet + Ru(bpy)_3^{3+} + H_2O,$$

$$BrO_2^\bullet + Ru(bpy)_3^{2+} + H^+ \rightarrow Ru(bpy)_3^{3+} + HBrO_2.$$

The bromous acid quickly reacts with bromide, reducing its concentration to the critical

value that allows the onset of the autocatalytic production of bromous acid [6, 13]. This causes the oscillator to fire, shortening the period of the oscillation in comparison with the natural period.

The inhibitory path involves the $Ru(bpy)_3^{2+*}$ reacting with bromomalonic acid, BrMa, to form bromide, Br^-, and the oxidized form of the catalyst, $Ru(bpy)_3^{3+}$ [1, 35–37]. The oxidized catalyst can then react further with BrMA to produce additional free bromide:

$$Ru(bpy)_3^{2+*} + BrMA \rightarrow Ru(bpy)_3^{3+} + Br^- + \text{other products},$$

$$Ru(bpy)_3^{3+} + BrMA \rightarrow Ru(bpy)_3^{2+} + Br^- + \text{other products}.$$

The bromide delays the firing of the oscillator by increasing the time it takes to reach its critical concentration necessary for the onset of the autocatalytic production of bromous acid.

The dominant pathway is dependent on the composition of the catalyst-free solution. In this study, we use the concentration of bromate in the catalyst-free solution to select the photochemical pathway. At high concentrations of bromate, the excitatory pathway is dominant, while at lower concentrations, the inhibitory pathway is dominant.

The excitatory and inhibitory responses of an oscillator to a perturbation in light intensity can be illustrated by constructing their respective phase response curves (PRCs). A PRC shows the change in phase of an oscillator due to a perturbation at a particular phase in its cycle [38, 39]. In the experimental system, this is achieved by perturbing the independent micro-oscillators at arbitrary phases with a light pulse and then recording the time of the next firing. The change in phase of a given oscillator is calculated as $\Delta\phi = 2\pi[T - (t_{i+1} - t_i)]/T$, where T is the natural period of the oscillator, and t_i and t_{i+1} are the occurrence times of the peaks prior to and following a perturbation, respectively. An interval of at least three periods between the perturbations is used, which allows the oscillators to relax back to their natural period. The natural period T of each oscillator is determined by measuring the period during its oscillatory cycle immediately prior to a perturbation. Figure 2 shows the results of the PRC experiments for both the hub and peripheral oscillators immersed in either excitatory or inhibitory catalyst-free solutions. Using the excitatory reaction mixture, both the hub and the peripheral oscillators have a phase resetting region in the latter half of their cycle, Fig. 2(a) and 2(c), which results in an almost immediate firing of an oscillator during

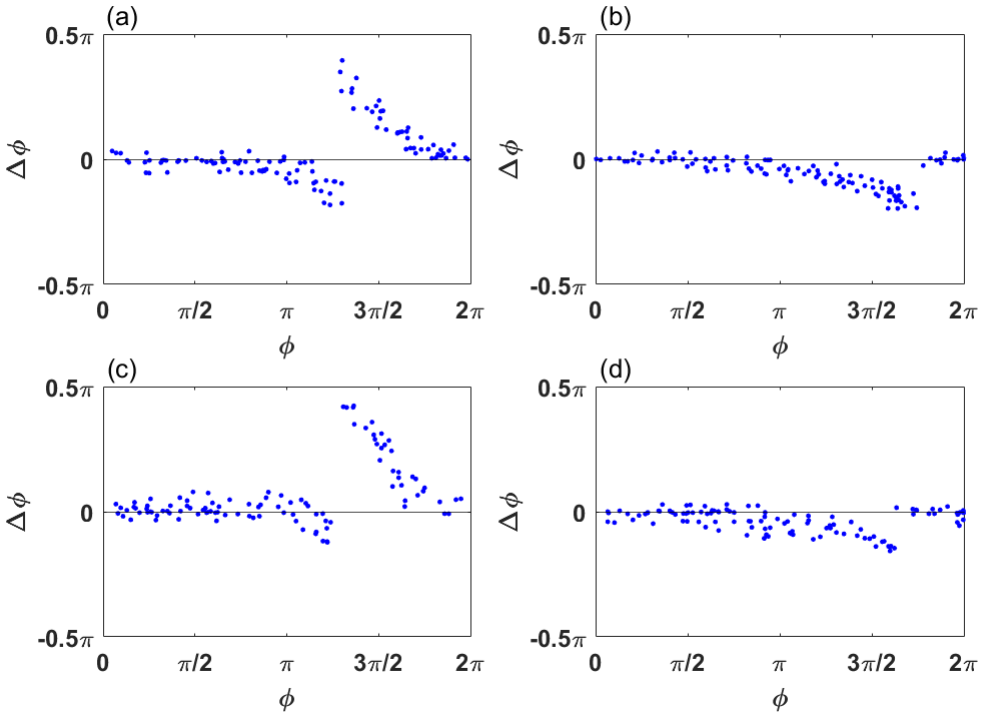

FIG. 2. Experimentally constructed phase response curves using excitatory or inhibitory reaction mixtures for hub and peripheral micro-oscillators. (a) PRC for the hub oscillators in an excitatory catalyst-free BZ reaction mixture showing both phase resetting and phase delaying regions. (b) PRC for the hub oscillators in an inhibitory catalyst-free BZ reaction mixture showing a phase delaying region. The PRCs for the peripheral oscillators are shown in panels (c) and (d) for excitatory and inhibitory catalyst-free BZ reaction mixtures, respectively.

a perturbation. Preceding the phase advancing regions are small phase delaying regions. Very early in its cycle, an oscillator is refractory and a perturbation therefore has minimal impact on its next firing time. When placed in an inhibitory catalyst-free BZ solution, both the hub oscillators, Fig. 2(b), and the peripheral oscillators, Fig. 2(d), exhibit only phase delays and refractory regions.

B. Experimental Results

When excitatory BZ micro-oscillators are coupled in a star network according to Eq. 1, two types of synchronization are observed. One has a single cluster of phase locked peripheral oscillators (1-cluster synchronization) and the other has two clusters of phase

locked peripheral oscillators (2-cluster synchronization), with several different occupancies. In both cases, the hub oscillator is not synchronized with the peripheral oscillators. To visualize the behaviors, the unwrapped phase of each oscillator is plotted as a function of time, as shown in Fig. 3. We see that the unwrapped phase plots of the peripheral

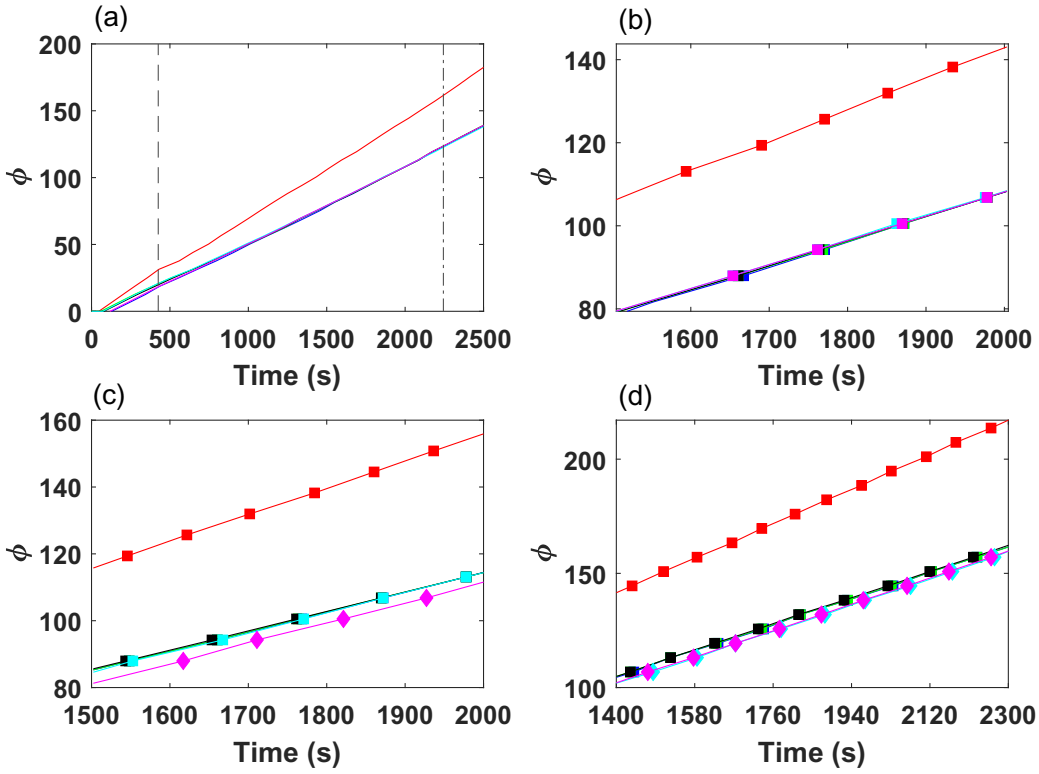

FIG. 3. The unwrapped phase of each oscillator as a function of time from experiments with excitatory coupling. (a) A 1-cluster synchronization state with the peripheral oscillators forming a single phase locked cluster. The dashed lines show when the coupling was switched on and switched off. (b) Detail of (a). (c) A 2-cluster synchronization state with 4-1 occupancy. The firing times for the cluster of 4 are indicated with squares, and those of the single oscillator are indicated with diamonds. (d) A two cluster state with 3-2 occupancy. The firing times for the cluster of 3 are indicated with squares, and those of the cluster of 2 are indicated with diamonds. In each plot, green, cyan, magenta or blue indicate peripheral oscillators and the red line indicates the hub oscillator. Initial concentrations of the catalyst-free BZ solution: $[BrO_3^-] = 0.640$, [MA] $= 0.096$, $[H^+] = 0.780$, and $[Br^-] = 0.0600$. The background light intensity was set to $\Phi_0 = 0.095$ mW cm^{-2}.

oscillators are parallel to each other, indicating that they are phase locked. With its higher frequency, the phase line of the hub diverges from phase lines of the the peripheral oscillators. Unwrapped phases of the individual oscillators for 1-cluster synchronization are shown in Figs. 3(a) and 3(b). Figures 3(c) and 3(d) show two different 2-cluster synchronization states involving different occupancies of the clusters. In both cases, the two clusters are

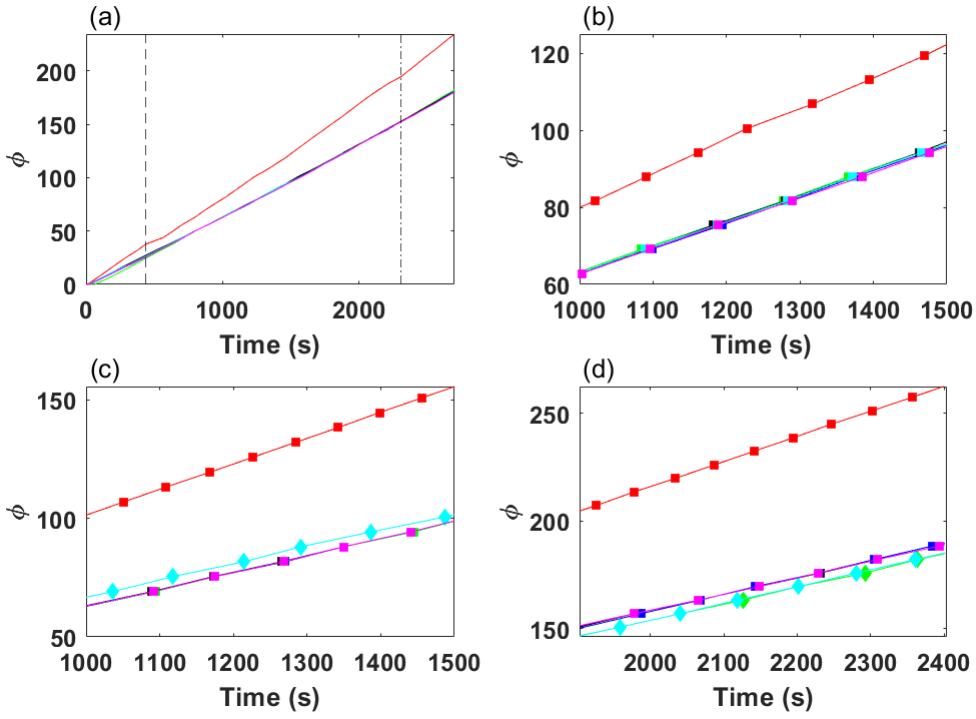

FIG. 4. The unwrapped phase of each oscillator as a function of time from experiments with inhibitory coupling. (a) A 1-cluster synchronization state with the peripheral oscillators forming a single phase locked cluster. The dashed lines show when the coupling was switched on and switched off. (b) Detail of (a). (c) A 2-cluster synchronization state having 4-1 occupancy. The firing times for the cluster of 4 are indicated with squares, and those of the single oscillator are indicated with diamonds. (d) A 2-cluster state with 3-2 occupancy. The firing times for the cluster of 3 are indicated with squares, and those of the cluster of 2 are indicated with diamonds. In each plot, green, cyan, magenta or blue indicate peripheral oscillators and the red line indicates the hub oscillator. Initial concentrations of the catalyst-free BZ solution: $[BrO_3^-] = 0.320$, $[MA] = 0.096$, $[H^+] = 0.780$, and $[Br^-] = 0.0600$. The background light intensity was set to $\Phi_0 = 0.081$ mW cm^{-2}.

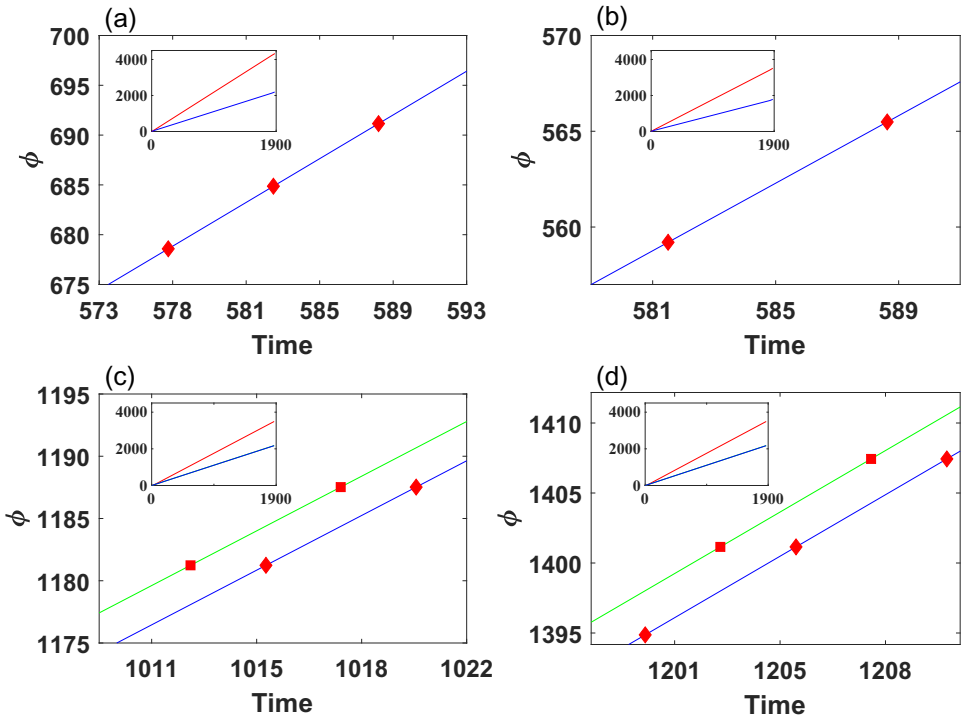

FIG. 5. Synchronization in star networks of coupled ZBKE oscillators in simulations (insets show long-term behavior). (a) Excitatory system and (b) inhibitory system. (c) Inhibitory system with a 2-cluster synchronization state having 4-1 occupancy. The firing times for the cluster of 4 are indicated with squares, and those of the single oscillator are indicated with diamonds. (d) Inhibitory system with a 2-cluster state having 3-2 occupancy. The firing times for the cluster of 3 are indicated with squares, and those of the cluster of 2 are indicated with diamonds. The natural period of the hub oscillator is 29.72, while the natural period of the peripheral nodes are equally spaced in the range of 44.36-44.95. Calculations are performed utilizing Euler's method with dt = 0.0019. Time is dimensionless in all simulations (Appendix A).

approximately antiphase to each other. Remarkably, very similar results are found in a star network of inhibitory oscillators. Figure 4 shows 1-cluster synchronization and two types of 2-cluster synchronization with inhibitory oscillators.

III. COMPUTATIONAL RESULTS

Computational studies of star networks are carried out using a modified three-variable ZBKE model [1, 4, 5, 40] to simulate each oscillator in the network. The model

incorporates a parameter, α, that determines the response of the photosensitive catalyst to light [1]. For $\alpha = 1$, an oscillator responds via the excitatory pathway, in which bromous acid is the critical product following the photoexcitation of the ruthenium complex. For $\alpha = 0$, an oscillator responds via the inhibitory channel, in which bromide is the critical product of the photoexcitation.

Computational phase response curves, based on the modified three-variable ZBKE model with either excitatory or inhibitory responses to light perturbations (see Appendix A), are in good agreement with the experimental phase response curves. Similarly, star networks of oscillators with either excitatory or inhibitory ZBKE oscillators exhibit essentially all of the behavior observed in the experiments. Figures 5(a) and 5(b) show 1-cluster synchronization states for the excitatory and inhibitory systems, respectively. Figures 5(c) and 5(d) show 2-cluster synchronization states in inhibitory systems with 4-1 and 3-2 occupancies, respectively. In all cases, the hub oscillator is not synchronized with the peripheral oscillators.

In the experimental system, we observe that different occupancies of 2-cluster states may occur for the same value of the coupling constant during different trials. Multistability is also seen in the ZBKE simulations. A particular cluster state at a given value of coupling strength can be targeted by the appropriate choice of the initial conditions. This is shown in Figs. 5(c) and 5(d), where using the same parameters as in 5(b) giving a 1-cluster state, 4-1 and 3-2 2-cluster synchronization states have been selected.

Figures 6(a) and 6(b) show the dominant behaviors at different coupling strengths from simulations of excitatory and inhibitory oscillators, respectively. In the case of excitatory oscillators, synchronization behavior is dominant at intermediate coupling strengths prior to the onset of global synchronization, Fig. 6(a). We have also observed global synchronization at large coupling strengths in the experimental system. In contrast, a star network of inhibitory oscillators exhibits oscillator death at higher coupling strengths, Fig. 6(b). The strong signal provided by the hub oscillator sufficiently delays the peripheral oscillators such that they do not have time to fire before receiving a second signal. This is predicted to occur at high coupling strengths corresponding to light intensities beyond those available in our experiments. Examples of global synchronization and oscillator death in ZBKE simulations are shown in Figs. 6(c) and 6(d), respectively.

During the transition from low coupling strength to the synchronized region and

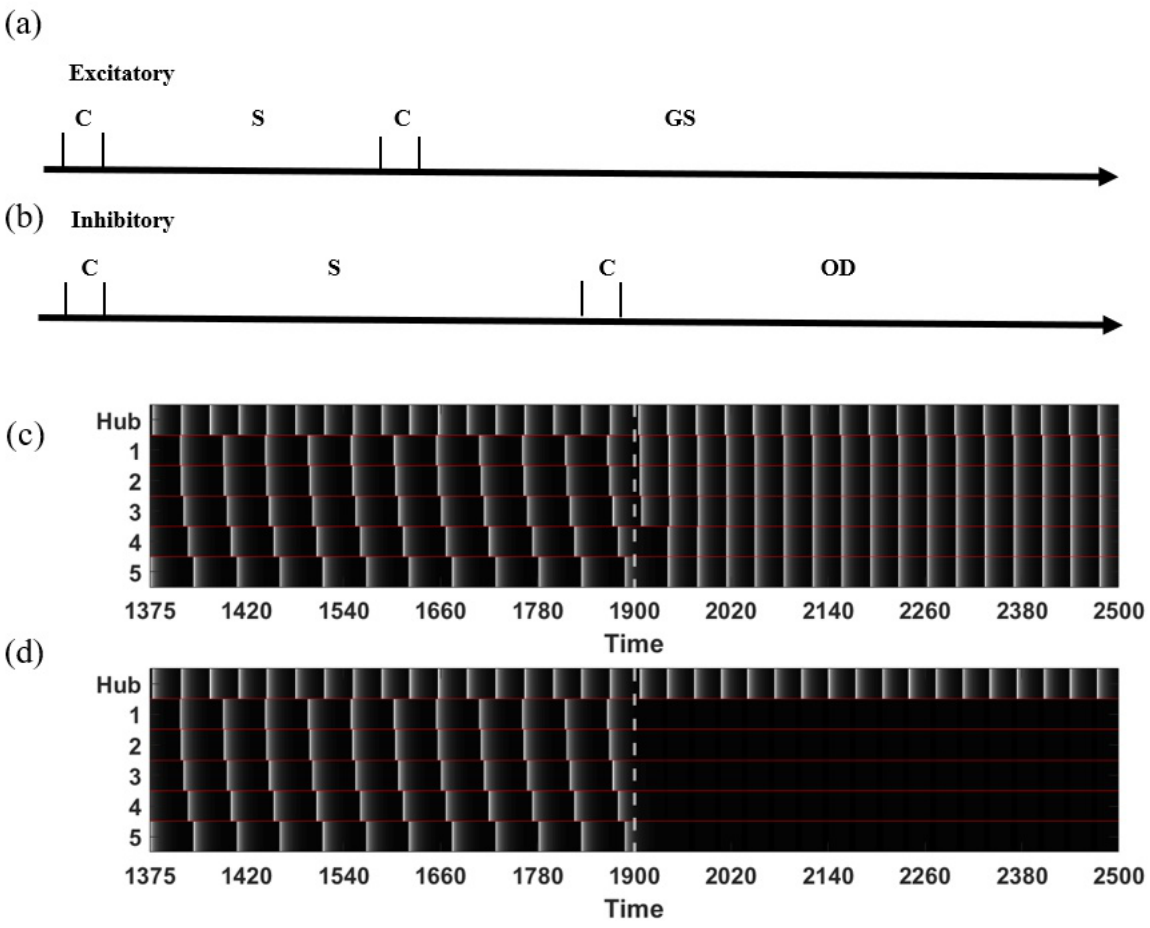

FIG. 6. Regions of behavior with increasing coupling strength in simulations of the excitatory system (a) and the inhibitory system (b): complex behavior (C), synchronization (S), global synchronization (GS), oscillator death (OD). Both 1-cluster and 2-cluster synchronization occurs across the entire (S) regions. (c) Global synchronization exhibited on increasing coupling strength from (S) region to GS region in (a). (d) Oscillator death exhibited on increasing coupling strength from (S) region to OD region in (b). Time is dimensionless in all simulations (Appendix A).

from the synchronized region to global synchronization or oscillator death, regions of complex behavior are found. Our investigations show that this complexity takes the form of high-order periodicity or aperiodic dynamics.

IV. DISCUSSION

In our studies of synchronization of BZ oscillators, we find that the coupling perturbation has little effect on the amplitude of the hub oscillations. It may, however, lead to significant changes in the timing of an oscillator firing, as illustrated by the PRCs shown in Fig. 2.

We now examine how the change in firing time leads to the 1-cluster and 2-cluster synchronization seen in our system. Figure 7(a) shows simulation results of a star network of excitatory photochemical oscillators. Coupling is initiated at 950 and, following a short transient, a repeating firing sequence of the oscillators is established. We see that the hub

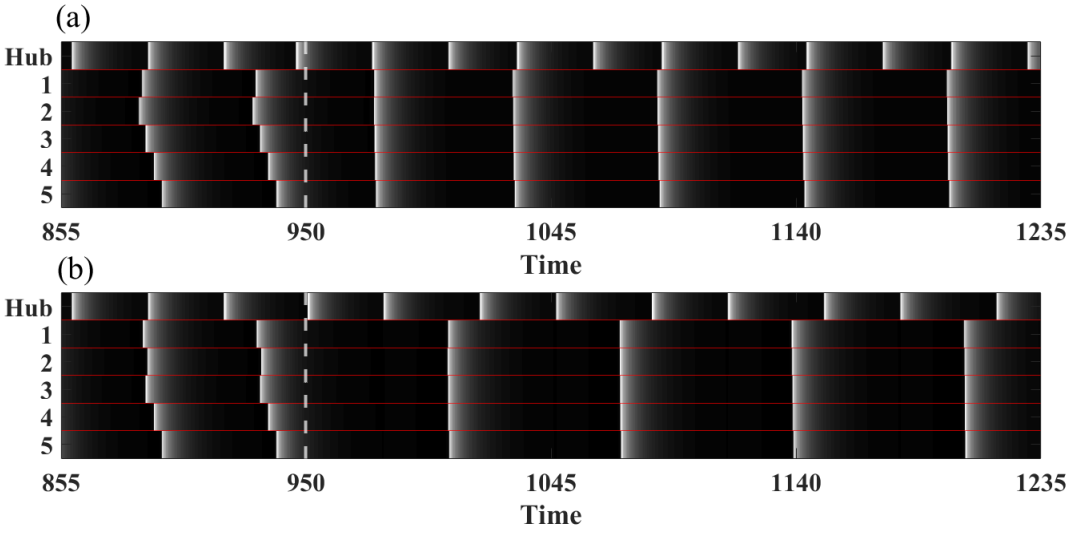

FIG. 7. (a) Firing sequence of single cluster state with excitatory coupling switched on at 950. The hub oscillator fires twice within the cycle of the peripheral oscillators, where the unperturbed cycle is the natural period of the hub. The perturbed cycle of the hub is shorter than the natural period due to the excitatory coupling. The peripheral oscillators 1-5 align in phase due to an inhibitory response to the perturbation from the hub. (b) Firing sequence of single cluster state with inhibitory coupling switched on at 950. The hub oscillator fires twice within the cycle of the peripheral oscillators, where the unperturbed cycle is the natural period of the hub. The perturbed cycle of the hub is longer than the natural period due to the inhibitory coupling. The peripheral oscillators 1-5 align in phase due to an inhibitory response to the perturbation from the hub. Time is dimensionless in all simulations (Appendix A).

fires twice during each cycle of the peripheral oscillators. The first firing occurs early in the refractory region of their cycle, while the second firing occurs when the peripheral oscillators are in the inhibitory portion of their cycle, and they are therefore each phase delayed. When they fire, they do so almost at the same time, and the hub is phase advanced. The hub then completes an unperturbed cycle and the firing sequence repeats.

The simulation shown in Fig. 7(b) demonstrates 1-cluster synchronization with inhibitory coupling. After a short transient, the same repeating firing sequence is established as in the excitatory system. In both cases, with excitatory or inhibitor oscillators, it is an inhibitory signal (phase delaying) from the hub that leads to the phase alignment of the peripheral oscillators. In both cases, the hub fires twice within the cycle of the peripheral oscillators, and in both cases the first signal has minimal impact because they are in their refractory period. The primary difference between the two systems is that the peripheral oscillators phase advance the hub in the excitatory system and phase delay the hub in the inhibitory system.

When a simulation is started with different initial conditions, a different firing sequence can be established and 2-cluster synchronization may be observed. A 3-2 two-cluster

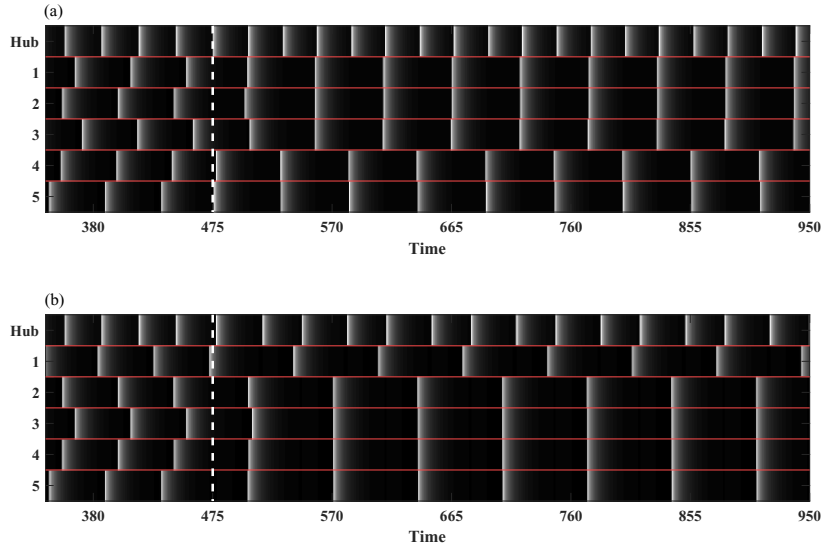

FIG. 8. Firing sequence of two cluster states with coupling switched on at 475. (a) A 3-2 two cluster state in an excitatory system, and (b) a 4-1 two cluster state in an inhibitory system. Time is dimensionless in all simulations (Appendix A).

state is shown in Fig. 8(a) for an excitatory system, and a 4-1 two-cluster state is shown in Fig. 8(b) for an inhibitory system. During 2-cluster synchronization, the firing sequence is the following: the hub fires, and then the first cluster fires, the hub fires again, and the second cluster fires. When the peripheral oscillators fire in the inhibitory system, the hub firing is delayed; however, when they fire in the excitatory system, the hub fires almost immediately and is phase advanced. The occupancy of the clusters is dependent on the initial conditions.

We can use the well defined sequence of firings of the oscillators during one-cluster synchronization to develop a map representation of the sequential firings and perturbations of the oscillators. This map can then be used to reveal the underlying dynamics that leads to synchronization. We use a minimal star network consisting of two peripheral oscillators and a hub oscillator. A schematic of their firing sequence is shown in Fig. 9. In the map representation, we assume that the response of each oscillator, following a perturbation at phase ϕ, can be determined directly from the PRC. The only exception to this is that the first perturbation the peripheral oscillators receive from the hub, during a given cycle, occurs too early to significantly impact their behavior. This perturbation is therefore ignored in the analysis. The order of firing of the peripheral oscillators, following the second perturbation by the hub, is based on the experiments and ZBKE simulations, with the faster oscillator (oscillator 1) always firing first. Since it fires first and is the faster oscillator, it must be receiving the perturbation from the hub at a phase, ϕ_1^i, later in its cycle than the phase, ϕ_2^i, at which the slower oscillator receives the perturbation. Figure 9 is representative of the inhibitory coupled single cluster state since the period of the hub on the perturbed cycle, T_h^i is larger than T_h^{nat}. In the excitatory system, the period of the hub on its perturbed cycle is less than T_h^{nat}. However, the sequence of firings are the same in the excitatory and inhibitory systems and the mapping approach is valid for both.

It is shown in Appendix B that by using a piecewise continuous approximation to the PRC, the time difference between successive firings is given by

$$t_{f2}^i - t_{f1}^i = \Delta T + (1 + Z')(t_{f2}^{i-1} - t_{f1}^{i-1}), \tag{2}$$

where $\Delta T = T_2 - T_1$, the difference in the natural periods of the two peripheral oscillators and t_{fj}^i is the time after the perturbation on the i-th cycle that oscillator j fires. Here, Z' is the slope of the linearly decreasing region of the piecewise continuous PRC. The fixed point

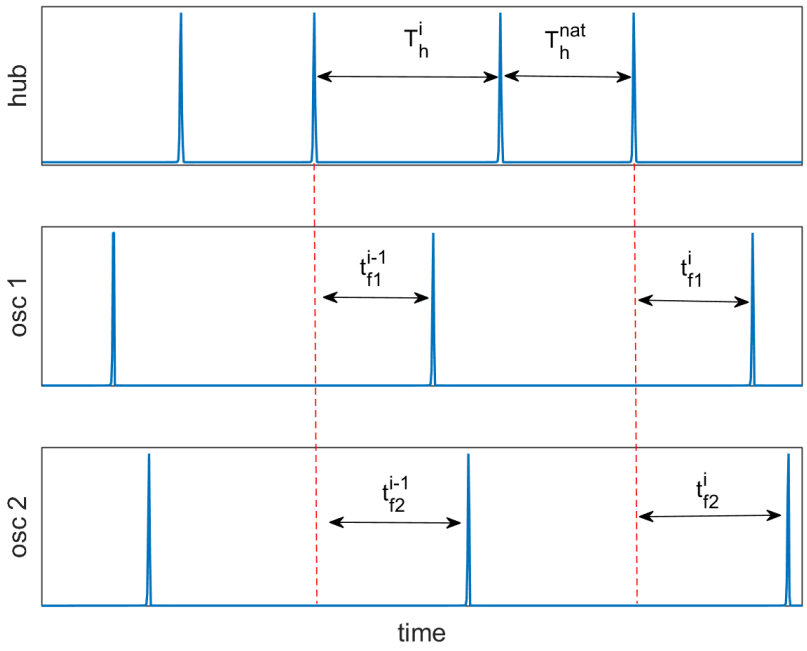

FIG. 9. Schematic map representation of the 1-cluster synchronization firing sequence for an inhibitory system. The hub oscillator fires twice for each cycle of the peripheral oscillators. The first firing of the hub is considered to have have no effect on the peripheral oscillators. On the *i-th* cycle, oscillator 1 receives the perturbation from the hub at phase ϕ_1^i and oscillator 2 receives the perturbation at phase ϕ_2^i.

of the map is given by

$$t_{f2} - t_{f1} = -\frac{\Delta T}{Z'}. \tag{3}$$

Stability analysis shows the fixed point to be stable for $-2 < Z' < 0$. Qualitatively, Eq. 3 can be interpreted as a competition between two processes, divergence and realignment. On any given cycle, the difference in their natural periods leads to the oscillators having different phase velocities that creates an initial divergence of their phases. The larger the difference in their natural periods the larger this divergence. Counteracting this on a given cycle, the perturbation from the hub acts to realign this divergence by delaying the faster oscillator more than the slower oscillator. This is guaranteed since both the real and piece-wise continuous PRCs are monotonically decreasing functions in the phase range of interest, with the faster oscillator always perturbed at a later phase. The net result of these two competing processes is the stable difference in the firing times of the two oscillators, Eq.

3.

We have observed in ZBKE simulations of both the inhibitory and excitatory coupled systems that at a given coupling strength there is a maximum heterogeneity, ΔT_{max}, above which synchronization is no longer observed. The mechanism for synchronization, as outlined above, requires that the divergence due to period heterogeneity is compensated for by delaying the faster oscillator more than the slower oscillator. In order for this to happen, oscillator 1 should be perturbed at a later phase than oscillator 2 but before ϕ_{crit}, where ϕ_{crit} corresponds to the abrupt decrease in the value of the inhibitory PRC close to 2π. If oscillator 1 were to be perturbed after ϕ_{crit}, it would be delayed less then oscillator 2. Therefore, the value of ϕ_1 must be within the range

$$\phi_2 < \phi_1 < \phi_{crit}. \tag{4}$$

As the phase velocity of oscillator 1 increases, relative to oscillator 2, the divergence between their pertubation phase will increase until eventually oscillator 1 is perturbed after ϕ_{crit}. Therefore, at some critical heteorgeneity we would no longer expect synchronization to occur.

While the above mapping approach was developed for the inhibitory system, we can use an equivalent approach to develop an understanding of synchronization in the excitatory system. The only difference is that the perturbation received by the hub from the peripheral oscillators results in it firing sooner than its natural period. Other than this, the firing sequence, see Fig. 9, and underlying competition between divergence and realignment of the peripheral oscillators by a later, in phase perturbation to the faster oscillator remains identical.

V. CONCLUSION

Our work reports on the identification of synchronization in a star network of coupled BZ chemical oscillators for both activatory and inhibitory coupling. Examination of the firing patterns in simulations shows that in both cases the synchronization of the peripheral oscillators arises via a delaying signal from the hub. Owing to the monotonically decreasing PRC, this acts to slow the faster oscillators more than the slower oscillators and aligns the firing times of the oscillators, Eq. 3. A maximum allowed heterogeneity for the existence of

synchronization is associated with the presence of the sharp transition in the PRC. If the faster oscillator fires at a phase later than this, it is no longer delayed more than the slow oscillator and their phases diverge. At higher coupling strengths, we see larger heterogeneity allowed due to stronger realignment of the faster oscillators relative to the slower oscillators. The minimal piece-wise linear PRC used in our mapping approach satisfies the condition that the PRC is a monotonically decreasing function of phase in the region where the oscillators are perturbed. For this reason, the mapping approach is able to reproduce much of the behavior seen in the more complex BZ system.

ACKNOWLEDGMENT

This material is based on work supported by the National Science Foundation, Grant No. CHE-1565665 and CHE-2102137.

APPENDIX A: COMPUTATIONAL STUDIES

Simulations are carried out using a modified three-variable ZBKE model [1, 4, 5, 40]. The photosensitive chemistry of oscillator j is described by the following:

$$\epsilon_1 \frac{dX_j}{dt} = \alpha\Phi_j - X_j^2 - X_j + \epsilon_2\gamma u_{ss}^2 + u_{ss}(1 - Z_j) + \mu Y_j - X_j Y_j, \tag{A1}$$

$$\epsilon_4 \frac{dY_j}{dt} = (1 - \alpha)\Phi_j - X_j Y_j - \mu Y_j + \frac{q_j \lambda Z_j}{\epsilon_3 + 1 - Zj} + \beta, \tag{A2}$$

$$\frac{dZ_j}{dt} = (1 + \alpha)\Phi_j + u_{ss}(1 - Z_j) - \frac{\lambda Z_j}{\epsilon_3 + 1 - Z_j}, \tag{A3}$$

where X_j, Y_j and Z_j represent [$HBrO_2$], [Br^-] and [$Ru(bpy)_3^{3+}$], respectively, and Φ_j is the light intensity. The steady state approximation of [$HBrO_2^+$] is represented as u_{ss}, with $u_{ss} = \frac{1}{4\gamma\epsilon_2}[Z_j - 1 + (16\gamma X_j\epsilon_2 + Z_j^2 - sZ_j + 1)^{\frac{1}{2}}]$. The nondimensional model parameters are $\epsilon_1 = 0.11$, $\epsilon_2 = 1.7 \times 10^{-5}$, $\epsilon_3 = 1.6 \times 10^{-2}$, $\epsilon_4 = 4.2 \times 10^{-4}$, $\gamma = 1.1$, $\lambda = 0.10$, $\beta = 1.7 \times 10^{-5}$, $\mu = 2.4 \times 10^{-4}$. The excitatory-inhibitory photochemical response of an oscillator is determined by the parameter α. When $\alpha = 1$, a light perturbation leads to production of $HBrO_2^+$, an excitatory response. When $\alpha = 0$, a light perturbation leads primarily to the production of bromide, an inhibitory response. Hub-peripheral oscillator period mismatch is introduced by variation in the stoichiometric coefficient, q_j, so that a hub oscillator has a natural period of 29.72 and the peripheral oscillators typically have periods within the

range of 44.36-44.95. This corresponds to an approximately 1.5% range in the period of the peripheral oscillators, similar to that seen in the experimental system.

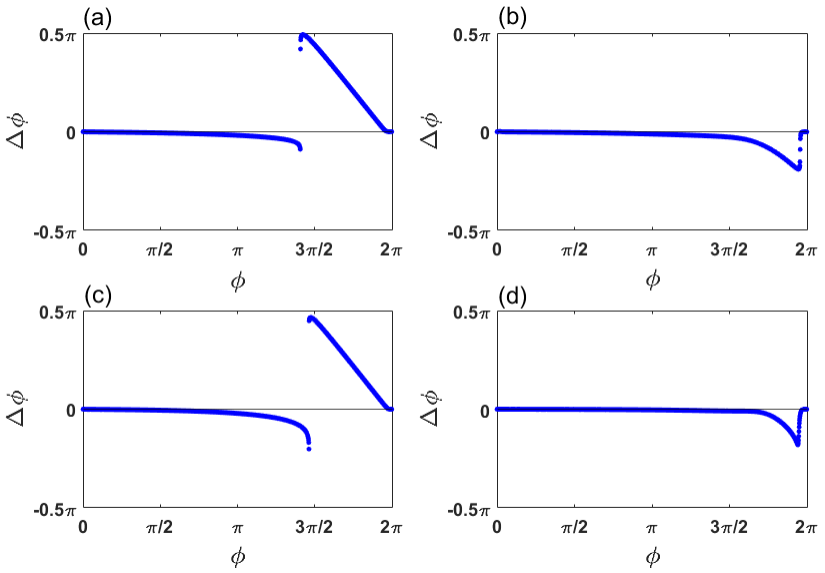

FIG. 10. Computational PRCs constructed using the modified three-variable ZBKE model. Panels (a) and (b) show the results for the hub oscillator using excitatory and inhibitory coupling, respectively. The peripheral oscillators are shown in panels (c) and (d) also using excitatory and inhibitory coupling, respectively.

Coupling of the oscillators is accomplished using the simulated light intensity, Φ, with

$$\Phi_j = \Phi_0 + \frac{K}{d}\sum_{i=1}^{N+1} A(Z_i - Z_j), \tag{A4}$$

where A is an adjacency matrix corresponding to a star network, $\Phi_0 = 0$, d is the degree of each node, and the coupling constant K ranges from 0 to 6.0×10^{-3}.

PRCs for the model system are constructed in a manner similar to the PRCs in the experimental system. A given oscillator is briefly perturbed through a change in the light intensity at a given phase and the impact on the timing of next firing is measured. This process is then repeated at all phases. The resulting PRCs for both the hub and peripheral oscillators are shown in Fig. 10 for the cases $\alpha = 1$ and $\alpha = 0$.

APPENDIX B: MAPPING APPROACH

A mapping description is developed for a star network consisting of a hub and two peripheral nodes. The natural periods of oscillator 1, 2 and the hub are T_1, T_2 and T_h^{nat}, respectively. Oscillator 1 and 2 receive a perturbation at phases ϕ_1 and ϕ_2, respectively. We assume that $T_2 > T_1$, $\phi_1 > \phi_2$ and ϕ_1 is subject to the constraints from Eq. 4.

The difference in firing times of the two peripheral oscillators following a perturbation is related to their phase synchronization. The map g of this difference in firing times acts on their previous cycles difference in firing times such that $t_{f2}^i - t_{f1}^i = g(t_{f2}^{i-1} - t_{f1}^{i-1})$.

The time of firing after perturbation of oscillator 1 on its *i-th* cycle is obtained directly from Fig. 9 as

$$t_{f1}^i = \frac{T_1}{2\pi}(2\pi - \phi_1^i - \Delta\phi_1^i),$$

with the change in phase, $\Delta\phi_1$, calculated using the PRC, $\Delta\phi_1 = Z(\phi_1)$,

$$t_{f1}^i = \frac{T_1}{2\pi}(2\pi - \phi_1^i - Z(\phi_1^i)).$$

To facilitate the development of the mapping approach, a piece-wise linear approximation to the PRC is made, as shown in Fig. 11(a). The phase response is defined to be zero between 0 and ϕ^* (for the definition of ϕ^* see Fig. 11(a)). $Z(\phi)$ then decreases linearly to a minimum value, at phase ϕ_{crit}, Fig. 11(a). Between phase ϕ_{crit} and 2π, the PRC is again defined to be zero. Z' is the slope of the linearly decreasing region of the piecewise continuous PRC. A larger (more negative) slope corresponds to a higher coupling strength in the ZBKE simulations. Figure 11(a) shows an example piece-wise linear approximation as well as the actual PRC. Also shown are two other PRCs generated using larger perturbations, i.e., corresponding to larger coupling strengths.

Here, we use the appropriate section of the piece-wise linear PRC, $Z(\phi) = Z'(\phi - 2\pi\frac{T_h^{nat}}{T_1})$, giving

$$t_{f1}^i = T_1 - \frac{T_1}{2\pi}(1 + Z')\phi_1^i + Z'T_h^{nat}.$$

If the phase at which oscillator 1 is perturbed,

$$\phi_1^i = \frac{2\pi}{T_1}((T_h^i + T_h^{nat}) - t_{f1}^{i-1})$$

is now substituted, and the time of firing after perturbation of oscillator 1 can be expressed

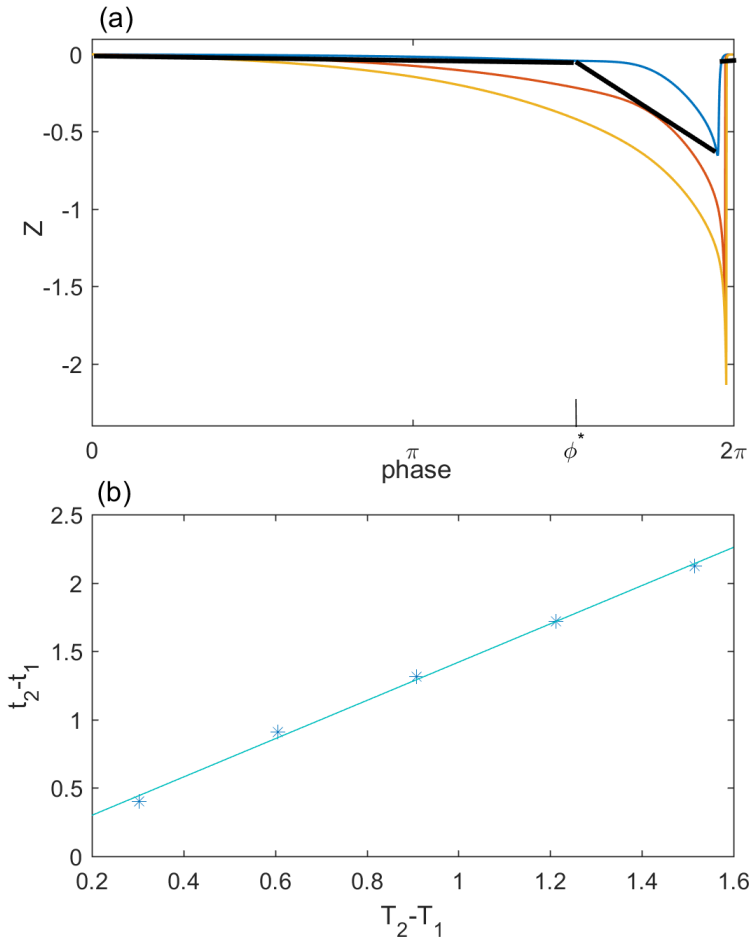

FIG. 11. (a) Three PRCs, blue line, red line and orange line, produced using an increasing size, respectively, of perturbation. A larger perturbation corresponds to a larger coupling strength in the coupled oscillator system. Black line: piece-wise linear representation of the blue line PRC. ϕ^* corresponds to $\frac{2\pi T_h^{nat}}{T_j}$ where T_j is the natural period of peripheral oscillator j. Examination of Fig. 9 shows that in the indicated firing sequence, a length of time of at least T_h^{nat} occurs before the peripheral oscillators are perturbed for the second time within their cycle. Therefore, for convenience the value of the PRC is set to 0 in the region, $0 \leq \phi \leq \phi^*$. (b) The dependence of firing time difference, $t_{f2} - t_{f1}$ following perturbation on the difference in natural periods (fixed coupling strength).

in terms of its time of firing on its previous cycle,

$$t_{f1}^{i} = T_1 - (1 + Z')(\tau - t_{f1}^{i-1}) + Z' T_h^{nat},$$

where $\tau = (T_h^i + T_h^{nat})$.
A similar expression for t_{f2}^{i} is given as

$$t_{f2}^{i} = T_1 - (1 + Z')(\tau - t_{f2}^{i-1}) + Z' T_h^{nat}.$$

Subtracting the difference in firing times gives the expression for the map g,

$$t_{f2}^{i} - t_{f1}^{i} = \Delta T + (1 + Z')(t_{f2}^{i-1} - t_{f1}^{i-1}).$$

Solving for the fixed point $t_{f2}^{i} - t_{f1}^{i} = t_{f2}^{i-1} - t_{f1}^{i-1}$ of this map results in Eq. 3.

This equation also predicts that the difference in firing times will increase as the heterogeneity, ΔT, in the system increases. Close examination of the ZBKE simulation, Fig. 7, shows that the oscillators do not fire at exactly the same phase and the phase difference between them increases as the difference in their natural periods increases. To illustrate this further, Fig. 11(b) shows the observed phase separation in a ZBKE simulation, consisting of a hub and two peripheral oscillator as ΔT increases. The difference in the firing times of the peripheral oscillators increases approximately linearly with ΔT as in Eq. 3.

DATA AVAILABILITY

The data that support the findings of this study are available from the corresponding author upon reasonable request.

[1] D. Yengi, M. R. Tinsley, and K. Showalter, "Autonomous cycling between excitatory and inhibitory coupling in photosensitive chemical oscillators," Chaos **28**, 045114 (2018).

[2] S. Nkomo, M. R. Tinsley, and K. Showalter, "Chimera states in populations of nonlocally coupled chemical oscillators," Phys. Rev. Lett. **10**, 244102 (2013).

[3] S. Nkomo, M. R. Tinsley, and K. Showalter, "Chimera and chimera-like states in populations of nonlocally coupled homogenous and heterogenous chemical oscillators," Chaos **26**, 094826 (2016).

[4] M. R. Tinsley, S. Nkomo, and K. Showalter, "Chimera and phase-cluster states in populations of coupled chemical oscillators," Nat. Phys. **8**, 662–665 (2012).

[5] A. Taylor, P. Kapetanopoulos, B. Whitaker, R. Toth, L. Bull, and M. R. Tinsley, "Clusters and switchers in globally coupled photochemical oscillators," Phys. Rev. Lett. **100**, 214101 (2008).

[6] J. F. Totz, R. Snari, D. Yengi, M. R. Tinsley, H. Engel, and K. Showalter, "Phase-lag synchronization in networks of coupled chemical oscillators," Phys. Rev. E **92**, 022819 (2015).

[7] J. F. Totz, J. Rode, M. R. Tinsley, K. Showalter, and H. Engel, "Spiral wave chimera states in large populations of coupled chemical oscillators," Nat. Phys. **14**, 282–285 (2018).

[8] A. Bergner, M. Frasca, G. Sciuto, A. Buscarino, E. J. Ngamga, L. Fortuna, and J. Kurths, "Remote synchronization in star networks," Phys. Rev. E **85**, 026208 (2012).

[9] L. V. Gambuzza, A. Cardillo, A. Fiasconaro, L. Fortuna, J. Gomez-Gardenes, and M. Frasca, "Analysis of remote synchronization in complex networks," Chaos **23**, 043103 (2013).

[10] B. Karakaya, L. Minati, L. V. Gambuzza, and M. Frasca, "Fading of remote synchronization in tree networks of Stuart-Landau oscillators," Phys. Rev. E **99**, 052301 (2019).

[11] J. Lacerda, C. Freitas, and E. Macau, "Multistable remote synchronization in a star-like network of non-identical oscillators," Appl. Math. Model. **69**, 453–465 (2019).

[12] V. Vlasov and A. Bifone, "Hub-driven remote synchronization in brain networks," Sci. Rep. **7**, 1–11 (2017).

[13] R. J. Field, E. Koros, and R. M. Noyes, "Oscillations in chemical systems. II. Thorough analysis of temporal oscillation in the bromate-cerium-malonic acid system." J. Am. Chem. Soc. **94**, 8649–8664 (1972).

[14] A. F. Taylor, "Mechanism and phenomenology of an oscillating chemical reaction," Prog. React. Kinetics Mech. **27**, 247–325 (2002).

[15] H. Markram, M. Toledo-Rodriguez, Y. Wang, A. Gupta, G. Silberberg, and C. Wu, "Interneurons of the neocortical inhibitory system," Nat. Rev. Neurosci. **5**, 793–807 (2004).

[16] S. Boccaletti, V. Latorab, Y. Morenod, M. Chavez, and D. U. Hwanga, "Complex networks: Structure and dynamics," Phys. Rep. **424**, 175 (2006).

[17] A. Arenas, A. Diaz-Guilera, J. Kurths, Y. Moreno, and C. Zhou, "Synchronization in complex networks," Phys. Rep. **469**, 93 (2008).

[18] C. Cherubini, S. Filipp, A. Gizzi, and A. Loppini, "Role of topology in complex functional networks of beta cells," Phys. Rev. E **92**, 042702 (2015).

[19] G. B. Ermentrout and C. C. Chow, "Modeling neural oscillations," Physiol. Behav. **77**, 629–633 (2002).

[20] L. M. Pecora, F. Sorrentino, A. M. Hagerstrom, T. E. Murphy, and R. Roy, "Cluster synchronization and isolated desynchronization in complex networks with symmetries," Nat. Commun. **5**, 1–8 (2014).

[21] F. Sorrentino, L. M. Pecora, A. M. Hagerstrom, T. E. Murphy, and R. Roy, "Complete characterization of the stability of cluster synchronization in complex dynamical networks," Sci. Adv. **2**, e1501737 (2016).

[22] J. D. Johnson and D. M. Abrams, "A coupled oscillator model for the origin of bimodality and multimodality," Chaos **29**, 073120 (2019).

[23] A. Barabási and A. Reka, "Emergence of scaling in random networks," Science **286**, 509 (1999).

[24] K. Albert and A. Barabási, "Statistical mechanics of complex networks," Rev. Mod. Phys. **74**, 47 (2002).

[25] M. Frasca, A. Bergner, J. Kurths, and L. Fortuna, "Bifurcations in a star-like network of Stuart-Landau oscillators," Intern. J. Bifur. Chaos **22**, 1250173 (2012).

[26] C. Meena, K. Murali, and S. Sinha, "Chimera states in star networks," Intern. J. Bifurc. Chaos **26**, 1–8 (2016).

[27] C. Xu, Y. Sun, J. Gao, W. Jia, and Z. Zheng, "Phase transition in coupled star networks," Nonlin. Dyn. **94**, 1267–1275 (2018).

[28] J. Gómez-Gardeñes, S. Gómez, A. Arenas, and Y. Moreno, "Explosive synchronization tran-

sitions in scale-free networks," Phys. Rev. Lett. **106**, 1–4 (2011).

[29] E. R. Kandel, J. H. Schwartz, and T. M. Jesssell, *Principles of Neural Science*, 4th ed. (McGraw-Hill Education, 2000).

[30] N. Brunel, "Dynamics of sparsely connected networks of excitatory and inhibitory spiking neurons," J. Comput. Neurosci. **208**, 183–208 (2000).

[31] D. Golomb and J. Rinzel, "Clustering in globally coupled inhibitory neurons," Physica D **72**, 259–283 (1994).

[32] M. M. Norton, N. Tompkins, B. Blanc, M. C. Cambria, J. Held, and S. Fraden, "Dynamics of reaction-diffusion oscillators in star and other networks with cyclic symmetries exhibiting multiple clusters," Phys. Rev. Lett. **123**, 148301 (2019).

[33] M. Toiya, V. K. Vanag, and I. R. Epstein, "Diffusivley coupled chemical oscillators in a microfluidic assembly," Agnew. Chem., Int. Ed. **47**, 7753–7755 (2008).

[34] M. Toiya, H. O. Gonzalez-Ochoa, V. K. Vanag, S. Fraden, and I. R. Epstein, "Synchronization of chemical micro-oscillators," J. Phys. Chem. Lett. **1**, 1241–1246 (2010).

[35] R. Toth and A. F. Taylor, "Review of the tris(2-2'-bipyridyl) ruthenium catalyzed Belousov-Zhabotinsky reaction," Prog. React. Kinet. Mech. **31**, 59–115 (2006).

[36] S. Kádár, T. Amemiya, and K. Showalter, "Reaction mechanism for light sensitivity of the $Ru(bpy)_3^{2+}$-catalyzed Belousov-Zhabotinsky reaction," J. Phys. Chem. A **101**, 8200–8206 (1997).

[37] Y. Mori, Y. Nakamichi, T. Sekiguchi, N. Okazaki, and T. Matsumura, "Photo-induction of chemical oscillation in the Belousov-Zhabotinsky reaction under the flow condition," Chem. Phys. Lett. **211**, 421–424 (1993).

[38] M. A. Netoff, T. Schwemmer and T. J. Lewis, *Experimentally estimating phase response curves of neurons:Theoretical and practical issues*, Phase Response Curves in Neuroscience: Theory, Experiment, and Analysis, Vol. 6 (Springer, New York, 2012) pp. 95–129.

[39] C. C. Canavier and S. Achuthan, *History of the Application of the Phase Resetting Curve to Neurons Coupled in a Pulsatile Manner*, Phase Response Curves in Neuroscience: Theory, Experiment, and Analysis, Vol. 6 (Springer, New York, 2012) pp. 73–91.

[40] A. M. Zhabotinsky, F. Buchholtz, A. B. Kiyatkin, and I. R. Epstein, "Oscillations and waves in metal-ion-cataylzed bromate oscillating reactions in highly oxidized states," J. Phys. Chem **97**, 7578–7584 (1993).